Energy Materials

Supplementary Materials

Online degradation estimation for hybrid supercapacitors via data-driven enhanced pseudo-two-dimensional model

Jun Liu[1,2,#], Jie Zhang[1,#], Xiongwei Wu[1,2,*], Shanguang lv[1], Xingrong Yin[1], Xuewen Wu[1], Chengyong Shu[3], Wei Tang[3], Jiabao Li[1], Bei Long[1,*]

[1]Hunan Engineering Technology Research Center of Vanadium Flow Battery and Energy Storage System, Hunan Province Yinfeng New Energy Co, Ltd., Changsha 410019, Hunan, China.

[2]College of Environment and Ecology, Hunan Agricultural University, Changsha 410128, Hunan, China.

[3]School of Chemical Engineering and Technology, Xi'an Jiaotong University, Xi'an 710049, Shannxi, China.

[#]These authors contributed equally to this work.

[*]**Correspondence to:** Prof. Xiongwei Wu, Hunan Engineering Technology Research Center of Vanadium Flow Battery and Energy Storage System, Hunan Province Yinfeng New Energy Co, Ltd., Changsha 410019, Hunan, China; College of Environment and Ecology, Hunan Agricultural University, Changsha 410128, Hunan, China. E-mail: wxw@hunau.edu.cn; Bei Long, Hunan Engineering Technology Research Center of Vanadium Flow Battery and Energy Storage System, Hunan Province Yinfeng New Energy Co, Ltd., Changsha 410019, Hunan, China. E-mail: longbei@xtu.edu.cn

ORCID: Xiongwei Wu (0000-0001-9393-7123), Bei Long (0000-0002-2258-1489)

The Supplementary materials include:

1. Nomenclature;

2. Pseudo-two-dimensions (P2D) of Hybrid supercapacitor;

3. Algorithm framework;

4. References.

1. Nomenclature

Nomenclature	
a	Electrode specific surface area (m^2/m^3)
c_e	Electrolyte lithium ion concentration (mol/m^3)
c_s	Solid-phase lithium ion concentration (mol/m^3)
$c_{s,\max}$	Maximum solid-phase lithium concentration (mol/m^3)
i_0	Exchange current density (A/m^2)
j_r	Interface reaction current density (A/m^3)
k	Reaction rate constant (m/s)
r	Particle radial position (m)
t	Time (s)
t_0^+	Lithium ion transference number
D_{ele}	Electrolyte diffusion coefficient (m^2/s)
D_s	Solid phase diffusion coefficient (m^2/s)
F	Faraday's constant (96485 C/mol)
R	Gas constant (8.314 J/(mol · K))
T	Temperature (K)
U	Open-circuit voltage (V)
α_a	Anodic transfer coefficient
α_c	Cathodic transfer coefficient
ε_e	Electrolyte volume fraction
η	Overpotential (V)
ϕ_e	Electrolyte potential (V)
ϕ_s	Solid-phase potential (V)
κ_{eff}	Effective electrolyte conductivity (S/m)
σ_{eff}	Effective solid-phase conductivity (S/m)

Abbreviated terms	
AI	Artificial Intelligence
ANN	Artificial Neural Networks
CEI	Cathode Electrolyte Interphase
CNN	Convolutional Neural Network
ECM	Equivalent Circuit Model
EDLC	Electric Double Layer Capacitor
EDL	Electric Double Layer
EIS	Electrochemical Impedance Spectroscopy
ele	Electrolyte
GPR	Gaussian Process Regression
HC	Hard Carbon
HSC	Hybrid Supercapacitors
IC	Incremental Capacity
MAPE	Mean Absolute Percentage Error
MSE	Mean Squared Error
ML	Machine Learning
NCM	Nickel-Cobalt-Manganese Oxide
neg	Negative Electrode
PINN	Physics-Informed Neural Networks
P2D	Pseudo 2D (Pseudo-Two-Dimensional)
P2D-CNN	Pseudo-Two-Dimensional-Convolutional Neural Network
pos	Positive Electrode
R^2	Coefficient of Determination
RMSE	Root Mean Square Error
RVM	Relevance Vector Machine
SEI	Solid Electrolyte Interphase
SOH	State of Health
SVM	Support Vector Machine

2. Pseudo-two-dimensions (P2D) of Hybrid supercapacitor

The electrochemical model of the hybrid supercapacitor established in this work is based on the extension of the P2D model proposed by Doyle, Fuller, & Newman [1], and is solved using Comsol 5.2. The parameter of the P2D model established in this work is shown Table S1. Some parameters were obtained through experimental testing, while the remaining ones were identified through Bayesian optimization parameter identification.

Table. S1 Parameter settings of the P2D model

Variable	Expression	Value	Describe
cs0_neg	cs_neg_max*0.02	597.5 mol/m^3 [i]	Initial negative electrode Li^+ concentration
i0ref_neg	10.05 [A/m^2]	10.05 A/m^2 [i]	Reference exchange current density of negative electrode
cs0_pos	cs_pos_max	31540.5 [i]	Initial positive electrode Li^+ concentration
i0ref_pos	13.4 [A/m^2]	13.4 A/m^2	Reference exchange current density of negative electrode
i_load	i_1C*C	64 A [m]	load current
i_1C	Q0*A/3600[s]	6.4 A [m]	1C discharge current
cl_0	2000[mol/m^3]	2048.6 mol/m^3 [i]	Initial electrolyte salt concentration
cycle_time	600[s]	600 s [m]	Charging and discharging cycle time
Q0	Cap/A	52127 C/m^2 [m]	Initial capacity
A	0.442[m^2]	0.442 m^2 [m]	Electrode area
Cap	6.4[A*h]	23040 C [m]	Capacity

cs_neg_max	29576.2 [mol/m^3]	29576.2 mol/m^3 [i]	Maximum lithium ion concentration of negative electrode
cs_pos_max	31540.5 [mol/m^3]	31540.5 mol/m^3 [i]	Maximum lithium ion concentration of positive electrode
epss_neg	1-epsl_neg	0.478 [i]	Solid phase volume fraction negative electrode
epss_pos	1-epsl_pos	0.52 [i]	Electrode volume fraction
L_Cu	9[um]	9E-6 m [m]	Copper length
L_Al	15[um]	1.5E-5 m [m]	Aluminum length
L_neg	100[um]	1E-4 m [m]	Negative electrode length
L_sep	16[um]	1.6E-5 m [m]	Separator length
L_pos	70[um]	7E-5 m [m]	Positive electrode length
brugl_pos	2.98	2.98 [i]	Positive electrode correction factor
brugl_sep	3.15	3.15 [i]	Separator correction factor
Av_pos	5.8914E5 [1/m]	5.8914E5 1/m [i]	Positive electrode active surface area
Av_neg	1.6457E5 [1/m]	1.6457E5 1/m [i]	Surface area
Sac_0	4.845e8[1/m]	4.845e8 1/m [i]	Double layer specific surface area
rp_neg	7[um]	7E-6 m [m]	Negative electrode particle radius
rp_pos	3[um]	3E-6 m [m]	Positive electrode particle radius
T	25[°C]	298.15 K [m]	Cell temperature

epsl_neg	0.35	0.35 [i]	Negative electrode porosity
epsl_pos	0.31	0.31 [i]	Positive electrode porosity
epsl_sep	0.370	0.37 [i]	Separator volume fraction
C	10	10 [m]	Charging rate
C_{dl}	0.578[F/m^2]	0.578 F/m^2 [i]	Electrical double-layer capacitor

* The superscript "i" represents the identification value, and the superscript "m" represents the measurement value.

3. Algorithm framework

3.1 CNN framework

This work implements the CNN model using the torch algorithm package [2]. The CNN model processes input data derived from incremental capacity (IC) curves, which specifically utilizing two channels corresponding to voltage (X-axis) and differential capacity (dQ/dV, Y-axis) of the IC curves, through a structured pipeline: it begins with four sequential convolutional blocks, each comprising a 1D convolutional layer (with 64/128/192/256 filters and kernel sizes 5/7/5/9 for blocks 1-4 respectively), a ReLU activation for non-linearity, 1D batch normalization for training stability, and 1D max pooling (kernel size 2) for downsampling. Following these blocks, global average pooling reduces feature map dimensionality to a fixed-length vector, which is then fed into a dense layer with 256 neurons—accompanied by ReLU activation and 35% dropout to prevent overfitting—before reaching the output layer that generates 10 task-specific parameters, including the State of Health (SOH) of the system and 9 key electrochemical parameters critical for performance assessment.
A detailed description of the CNN architecture, together with key hyperparameters including learning rate, number of epochs, batch size and optimizer, has been summarized in Table. S2.

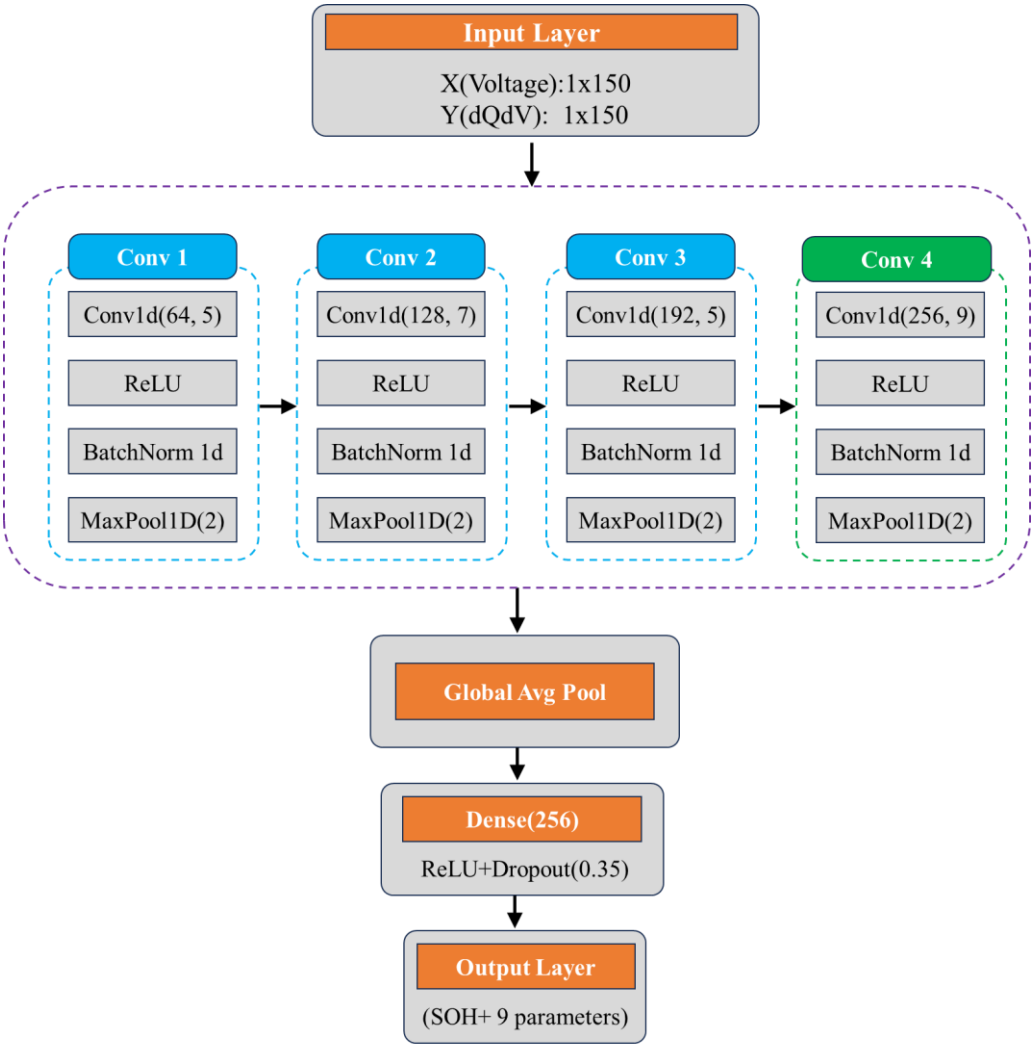

Fig. S1 CNN framework setting in this work

Table. S2 Summary of Key Hyperparameters for the CNN Model

Hyperparameter Category	Parameter Name	Value/Settings
Model Architecture	Number of convolutional layers	4
	Filters / Kernel size (Conv1)	64 filters, 5×1 kernel
	Filters / Kernel size (Conv2)	128 filters, 7×1 kernel

Hyperparameter Category	Parameter Name	Value/Settings
	Filters / Kernel size (Conv3)	192 filters, 5×1 kernel
	Filters / Kernel size (Conv4)	256 filters, 9×1 kernel
	Neurons in fully connected layer	256
	Dropout rate	0.35
	Output dimension	10 (9 electrochemical parameters and SOH value)
Optimizer Configuration	Optimizer type	Adam
	Initial learning rate (pre-training)	3.4814×10^{-4}
	Weight decay (pre-training)	3.0×10^{-4}
	Learning rate (fine-tuning)	1.0×10^{-5}
	Weight decay (fine-tuning)	1.0×10^{-5}
Training Process	Batch size (pre-training)	64
	Batch size (fine-tuning / prediction)	16 (fine-tuning) / 32 (prediction)
	Training epochs (pre-training)	200 (early stopping: terminate if no validation loss improvement for 15

Hyperparameter Category	Parameter Name	Value/Settings
		epochs)
	Training epochs (fine-tuning)	50
	Learning rate scheduler (pre-training)	ReduceLROnPlateau (factor=0.5, patience=10, min_lr=1e-6)
	Loss function	Mean Squared Error (MSE)

3.2 Uniqueness Verification of the IC Curve

To prove the uniqueness of the mapping of the IC curve to the electrochemical state, we conducted an inverse model verification. As shown in Fig. S2, randomly generated 100 sets of electrochemical parameters, generated the IC curve through the P2D model, then imported this IC curve into the neural network system for parameter identification. The identified parameters were then imported back into the P2D model to calculate the IC curve. The comparison between the initial IC curve and the reversed model IC curve is shown in Fig. S3. Note that the 4 curves were randomly selected from 100 sets of data. It can be seen that the IC curve fits well, with only minor differences, the main features are basically the same, which proves the uniqueness of the electrochemical state and the fact that the machine model is constrained by physical models.

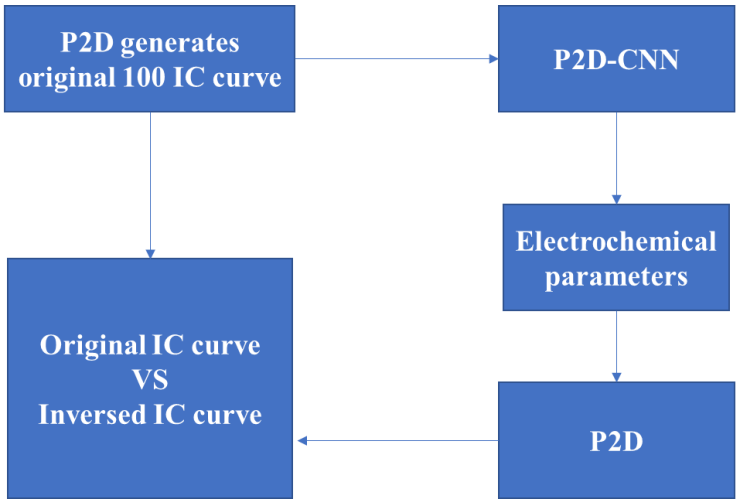

Fig. S2 Verification steps of the inverse model.

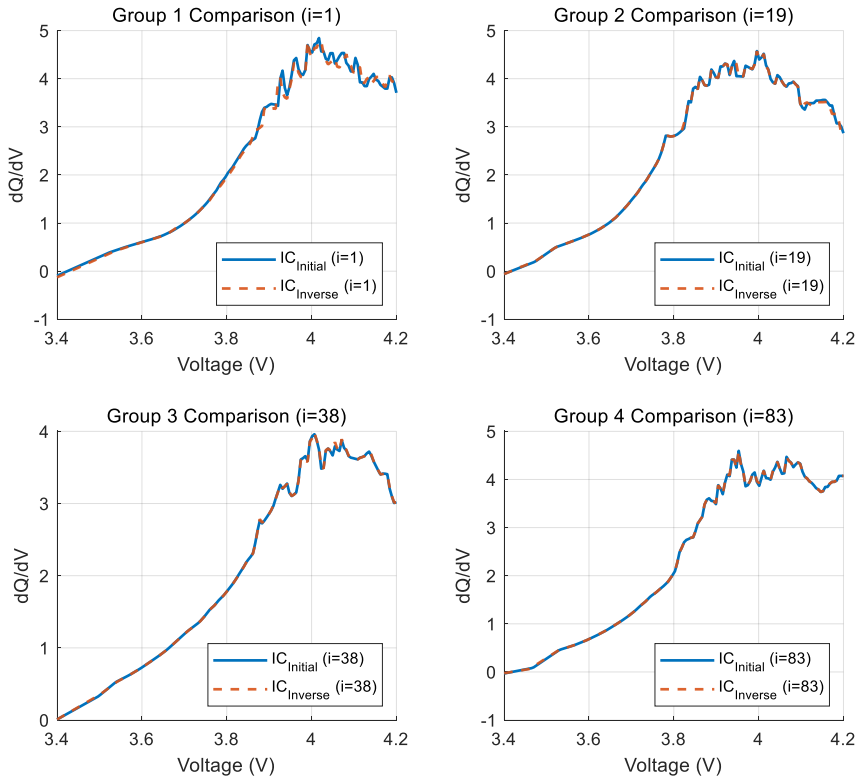

Fig.S3 Comparison of the IC curves between the initial model and the reverse model.

3.3 Identification of internal resistance changes

To quantitatively demonstrate the synthetic parameter space realistically reflects true degradation trajectories of hybrid supercapacitors under high-rate cycling, the internal resistance prediction of P2D-CNN was carried out and compared with the experimental data. Firstly, the electrochemical parameters are predicted using the IC

curve through the P2D-CNN program, and these electrochemical parameters are then imported into the P2D model for finite element simulation calculation. A small direct current pulse was applied under steady-state conditions, and the equivalent resistance was calculated as R_{DC}=ΔV/I. The simulated internal resistance integrates ohmic resistance, charge-transfer resistance and diffusion impedance inherently described in the P2D model.

The calculated internal resistance was compared with the experimental internal resistance as shown in Fig. S4. It can be seen that the predicted trend is highly consistent, with the result error within 10%. This is sufficient to demonstrate that the predicted electrochemical parameters have clear physical significance and can truly reflect the electrochemical degradation process.

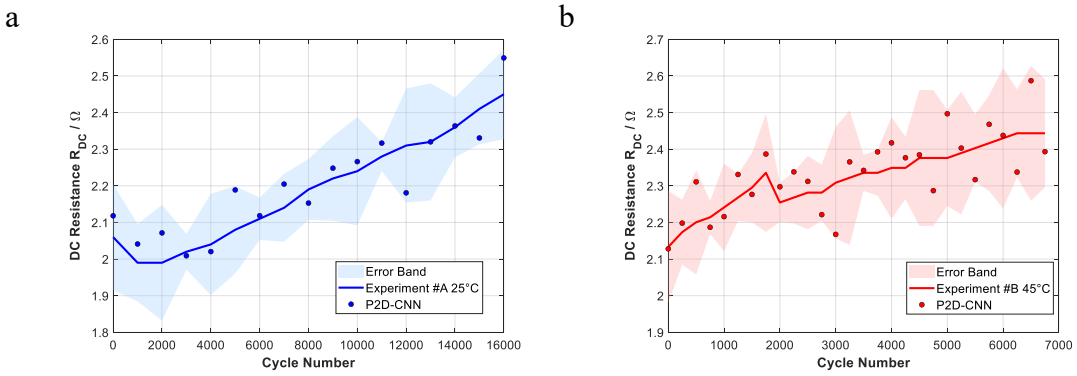

Fig. S4 Comparison between experimental measurements and simulated values of DC internal Resistance

3.4. Data processing and robustness testing

The IC curves were processed through a robust workflow: We first extracted valid charging-segment data, then performed noise-controlled numerical differentiation to avoid abnormal spikes, applied adaptive Savitzky–Golay smoothing to retain electrochemical features, used a fixed voltage grid for unified interpolation, and carried out simultaneous outlier removal for both IC and SOH data. These steps effectively suppress measurement noise, reduce errors from limited voltage resolution,

and ensure stable curve features under reasonable smoothing adjustments. As a result, the key characteristic peaks of IC curves and the corresponding parameter identification results remain highly consistent and stable, fully verifying the reliability and robustness of our processing method.

A robustness validation was conducted to demonstrate the parameter identification results remain highly stable under measurement noise and voltage resolution limits. As illustrated in Fig. S5, random voltage data loss was simulated and the incomplete data were reconstructed via nearest neighbor interpolation. A comparison of the prediction results between the original and reconstructed datasets are shown in Fig. S6. It can be seen that the prediction outputs exhibit no significant deviation even at a 10% data missing ratio. This is sufficient to demonstrate that our data processing method has excellent stability.

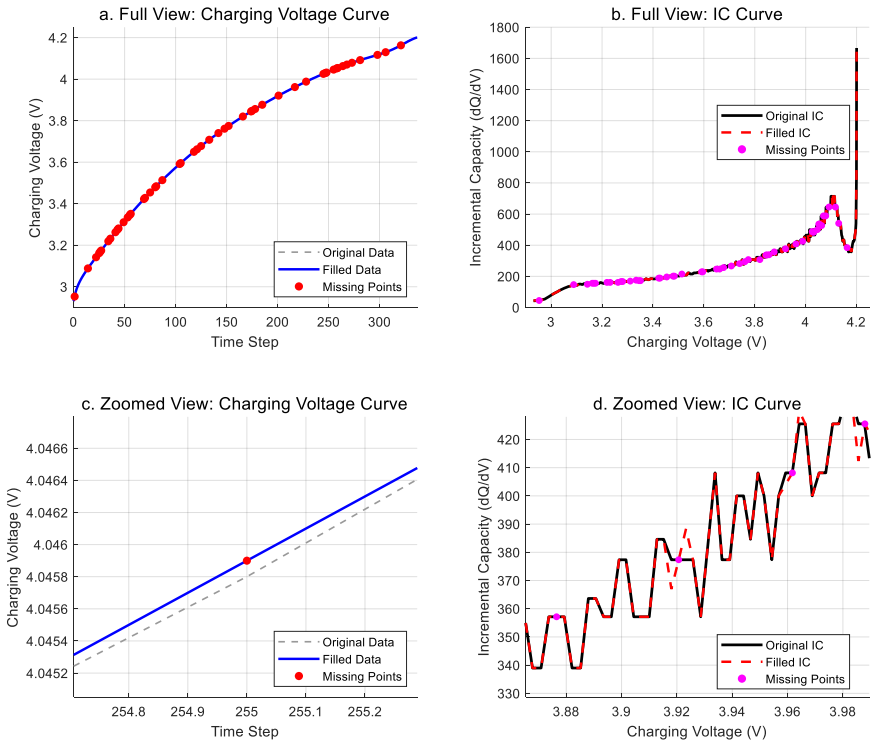

Fig. S5 The generation and processing method of the defective IC curve.

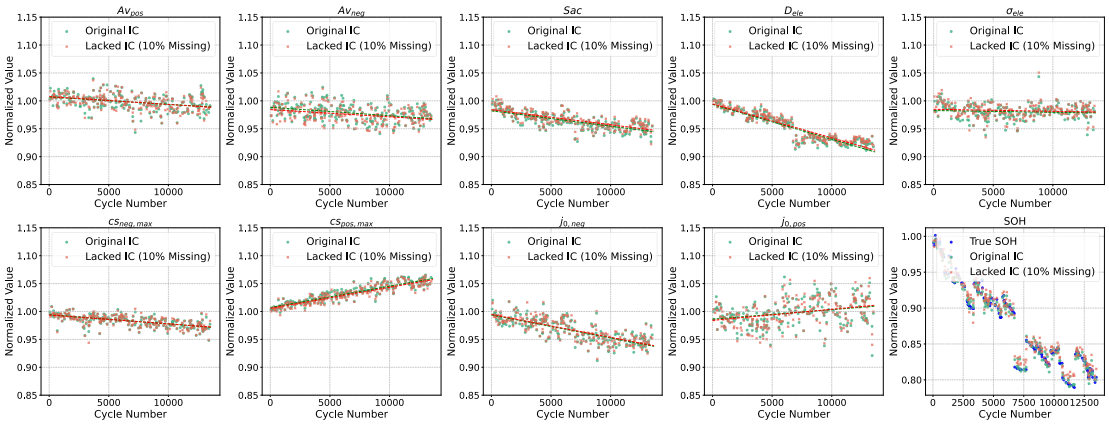

Fig. S6 Parameter identification in the case of missing IC curve data.

3.5. Fine-tuning framework

The fine-tuning model framework used in this work is shown in the Fig. S7. First, a CNN model trained on the #A dataset is used as the basis, and this model has learned general features related to HSC aging (such as the mapping relationship between IC curves and electrochemical parameters). Subsequently, the IC curve data of #B undergoes the same preprocessing procedure as that of #A (standardization and dimension reshaping) to ensure the consistency of input distribution, while focusing on optimizing the SOH prediction task for # B. In the fine-tuning phase, early-stage data is selected to construct the fine-tuning dataset so as to cover the initial aging features; the model parameters are frozen, with only the top classifier layers trainable, so as to avoid damaging the general feature extraction ability obtained from pre-training; the loss function only calculates the SOH prediction loss to achieve targeted optimization of key indicators; a small learning rate of 1e-5 is adopted for fine-tuning to prevent overfitting on the new dataset. By retaining the feature extraction ability of the pre-trained model and adjusting a small number of parameters to adapt to the characteristics of #B, the migration from a general model to a dedicated model is completed.

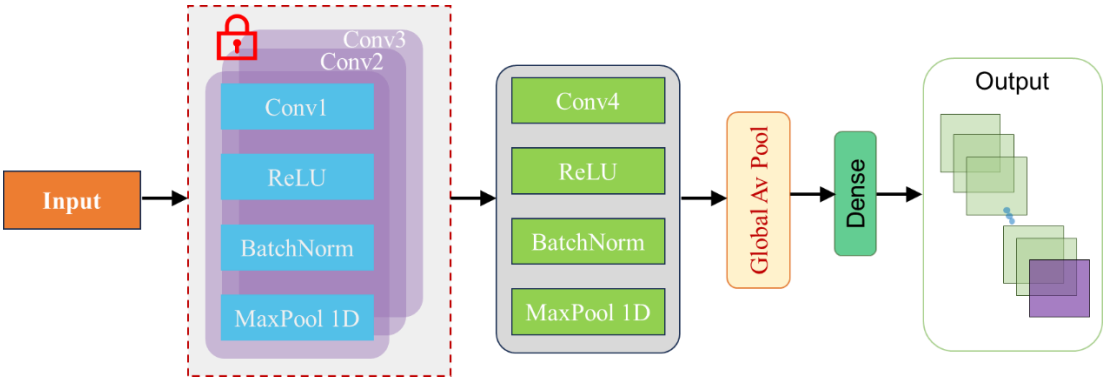

Fig.S7 Migration learning flowchart.

To further verify the transferability of the proposed method, we have generated additional data under new operating conditions using the calibrated P2D model and performed transfer learning tests. As illustrated in Fig. S8 and Fig. S9, this approach still achieves high-precision prediction via fine-tuning with only 10% of the cycle data in these new scenarios.

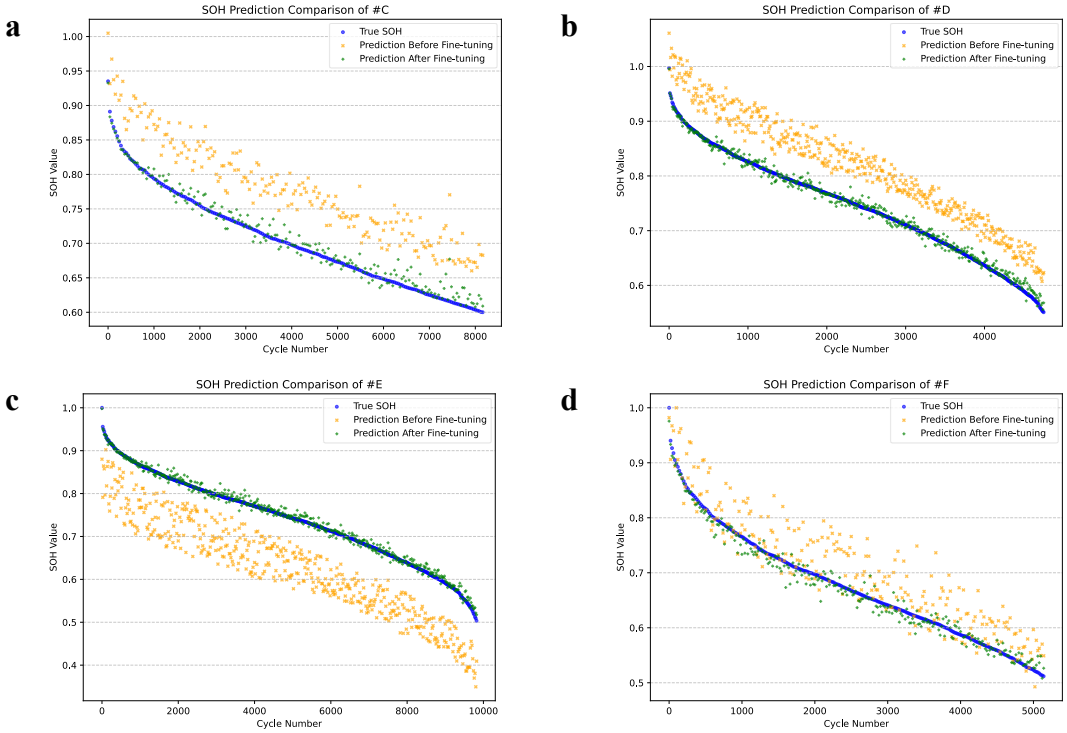

Fig. S8 The SOH prediction results after transfer learning on different battery model datasets.

a

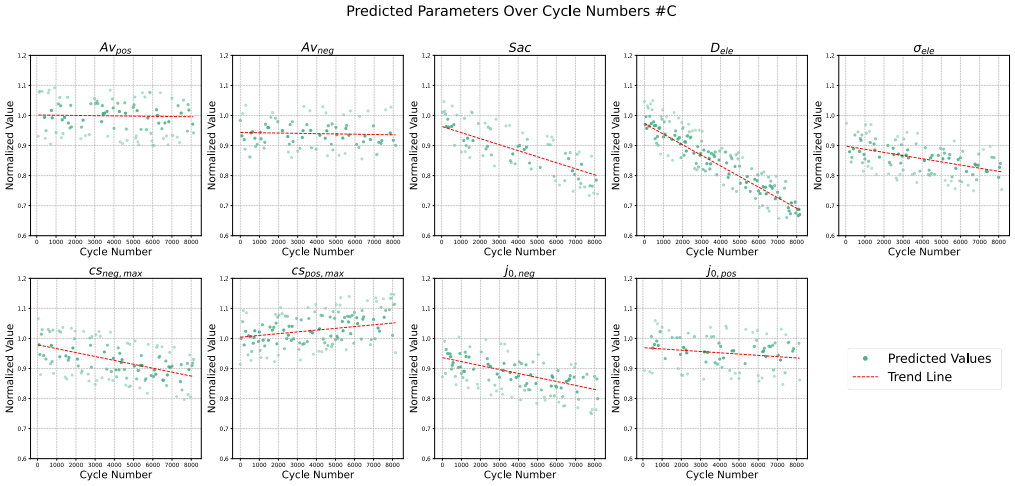
Predicted Parameters Over Cycle Numbers #C
Av_{pos}
Av_{neg}
Sac
D_{ele}
σ_{ele}
$cs_{neg,max}$
$cs_{pos,max}$
$j_{0,neg}$
$j_{0,pos}$
Normalized Value
Cycle Number
Predicted Values
Trend Line

b

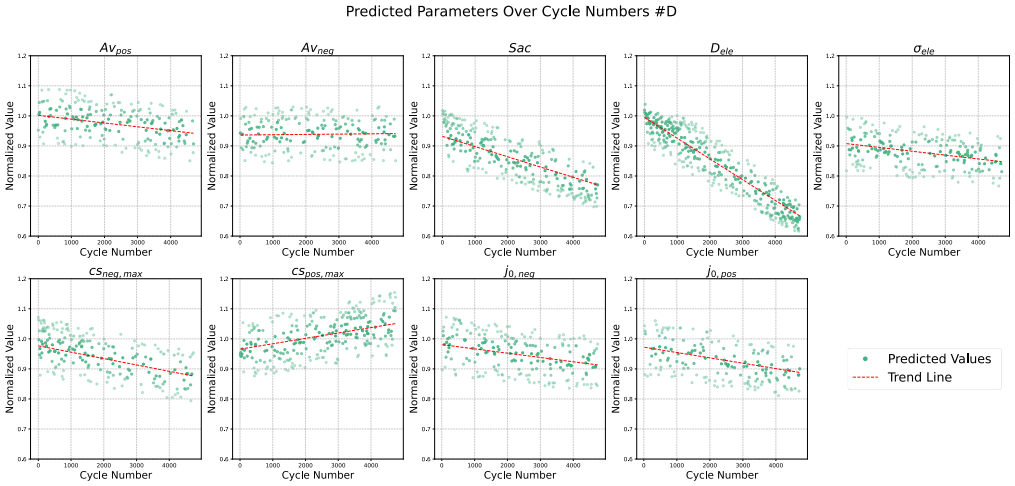
Predicted Parameters Over Cycle Numbers #D
Av_{pos}
Av_{neg}
Sac
D_{ele}
σ_{ele}
$cs_{neg,max}$
$cs_{pos,max}$
$j_{0,neg}$
$j_{0,pos}$
Normalized Value
Cycle Number
Predicted Values
Trend Line

c

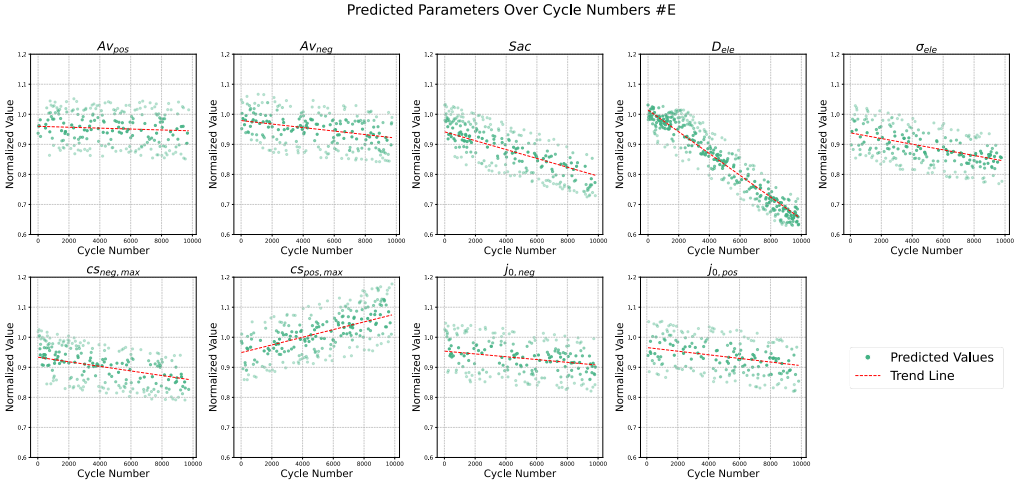
Predicted Parameters Over Cycle Numbers #E
Av_{pos}
Av_{neg}
Sac
D_{ele}
σ_{ele}
$cs_{neg,max}$
$cs_{pos,max}$
$j_{0,neg}$
$j_{0,pos}$
Normalized Value
Cycle Number
Predicted Values
Trend Line

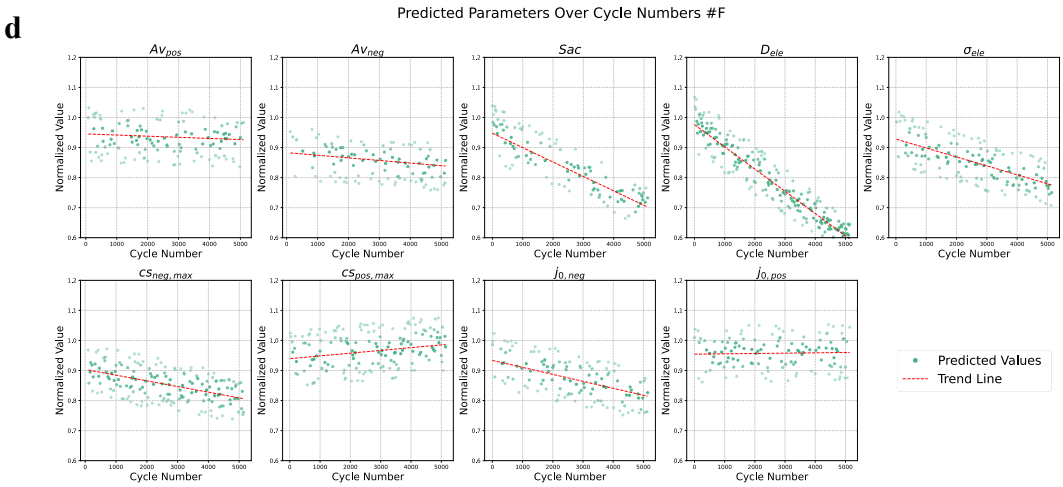

Fig. S9 The electrochemical parameter prediction results after transfer learning on different battery model datasets.

References

[1] Fuller, Thomas F .Simulation and Optimization of the Dual Lithium Ion Insertion Cell[J].Journal of the Electrochemical Society, 1994, 141(1):1.DOI:10.1149/1.2054684.

[2] Paszke, Adam et al. “PyTorch: An Imperative Style, High-Performance Deep Learning Library.” ArXiv abs/1912.01703 (2019): n. pag.